Supporting Information For:

Room-Temperature Electron-Selective Passivating Contact with Titanium-Peroxo Complexes for High-Efficiency Silicon Solar Cells

AUTHOR NAMES

Naser Beyraghi, Gence Bektaş, Doguscan Donmez, Mohammad Dehnavi, Daming Chen, Yifeng Chen, Zhiqiang Feng, Hui Shen, Gorkem Gunbas, Selcuk Yerci**

E-mail: syerci@metu.edu.tr

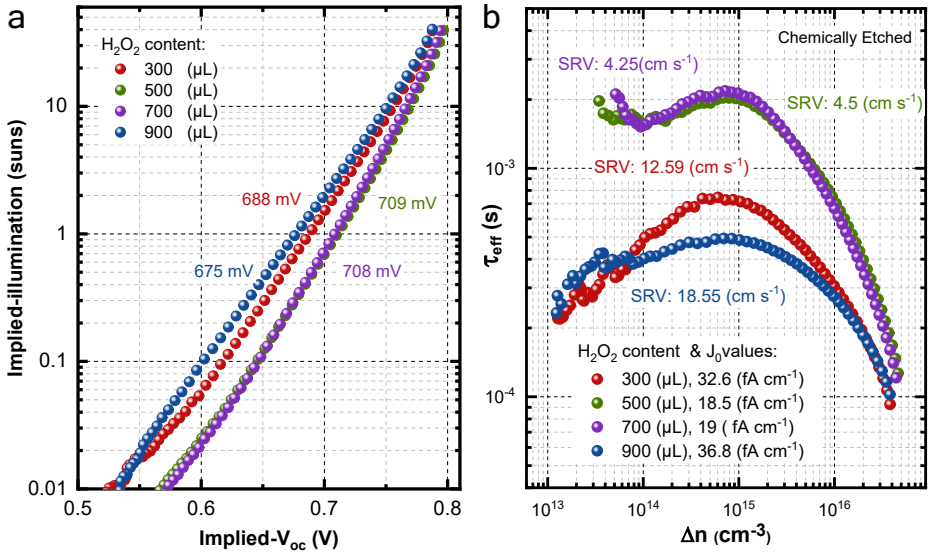

Figure S1. a) Implied open- circuit voltage (iV_{oc}) measured for varying sun illuminations. The iV_{oc} values written in the figure are extracted at 1 sun. b) Effective excess carrier lifetime (τ_{eff}) versus excess carrier concentration (Δn). The corresponding surface recombination velocity (SRV) and the recombination current density (J_0) extracted at high injection level are displayed next to each curve and in the legend, respectively. (All the passivation samples were prepared on HF-pretreated chemically etched (CZ) n-type c-Si substrates (1–3 Ω cm, 180 µm)).

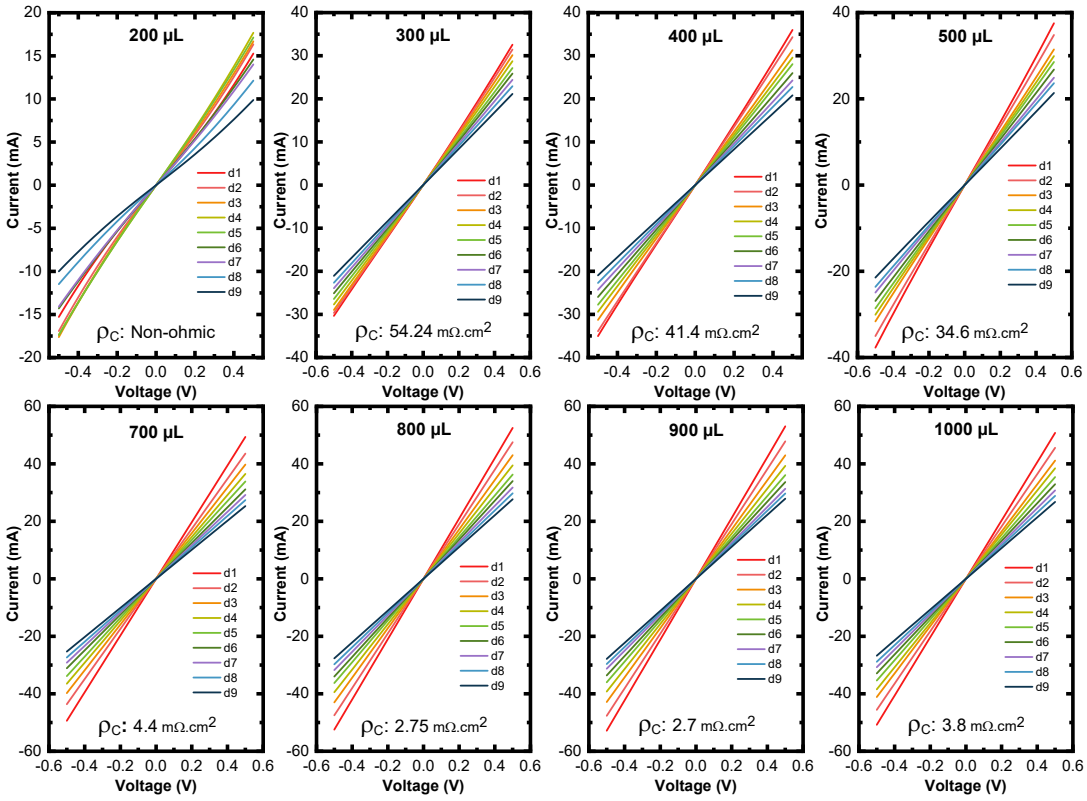

Figure S2. Dark current–voltage (I–V) curves and the extracted mean contact resistivity of the TLM test samples fabricated by M-TiO_x precursor solutions with different H_2O_2 contents. (All the samples were prepared on HF-pretreated chemically etched (CZ) n-type c-Si substrates (1–3 Ω cm, 180 µm)).

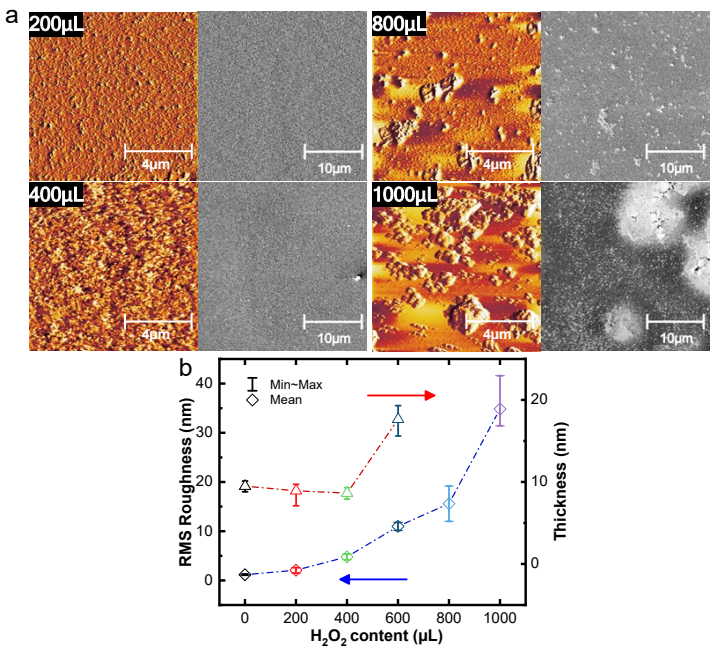

Figure S3. a) AFM and SEM images of the spin-coated layers fabricated by M-TiO_x precursor solutions with different H_2O_2 contents. b) Corresponding variation range in the surface RMS roughness and the layer thickness. (All samples were prepared on HF-pretreated CZ-DSP n-type c-Si substrates)

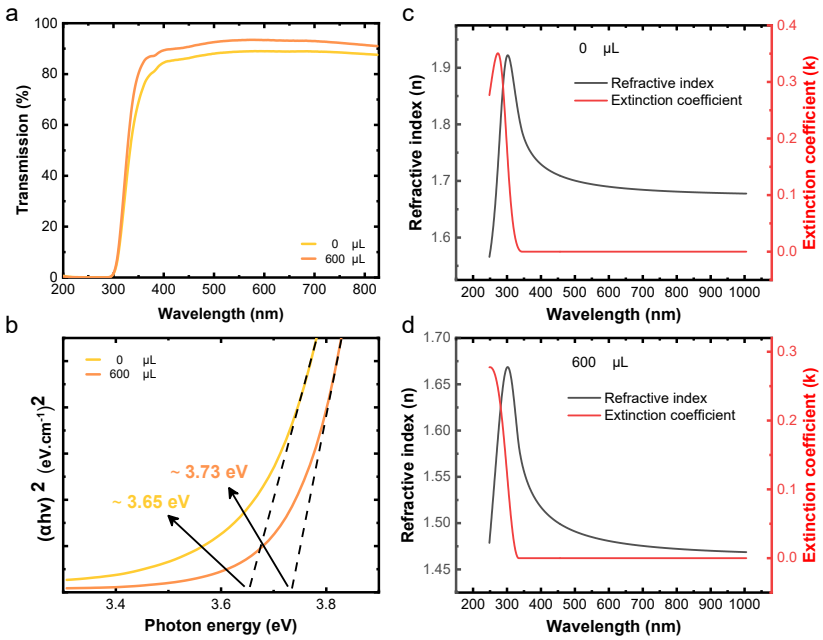

Figure S4. Of unmodified and modified layers, (a) UV-Visible transmission spectra (b) Tauc-plot optical bandgap, (c) and (d) refractive index (n) and extinction coefficient (k) spectra.

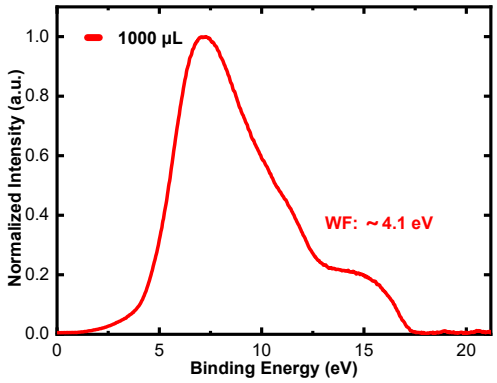

Figure S5. UPS spectra of the sample coated with a precursor solution containing 1000 µL of H_2O_2.

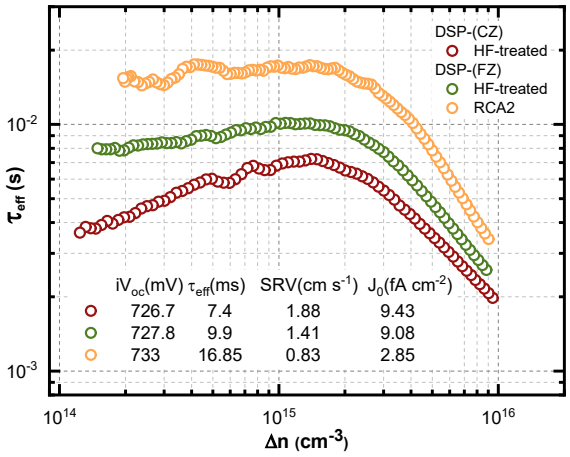

Figure S6. The effective excess carrier lifetime (τ_{eff}) versus excess carrier concentration (Δn) of DSP passivation test samples symmetrically coated by M-TiO_x precursor solution. The H_2O_2 content in M-TiO_x solution is 400 µL and 600 µL for RCA2 and HF pretreated samples, respectively. (The passivation substrates were n-type c-Si (1–3 Ω cm, 280 µm)). (note that J_0 values correspond to the accumulated saturation current density of the symmetric passivation test samples and must be divided by two to obtain single-side J_0 value).

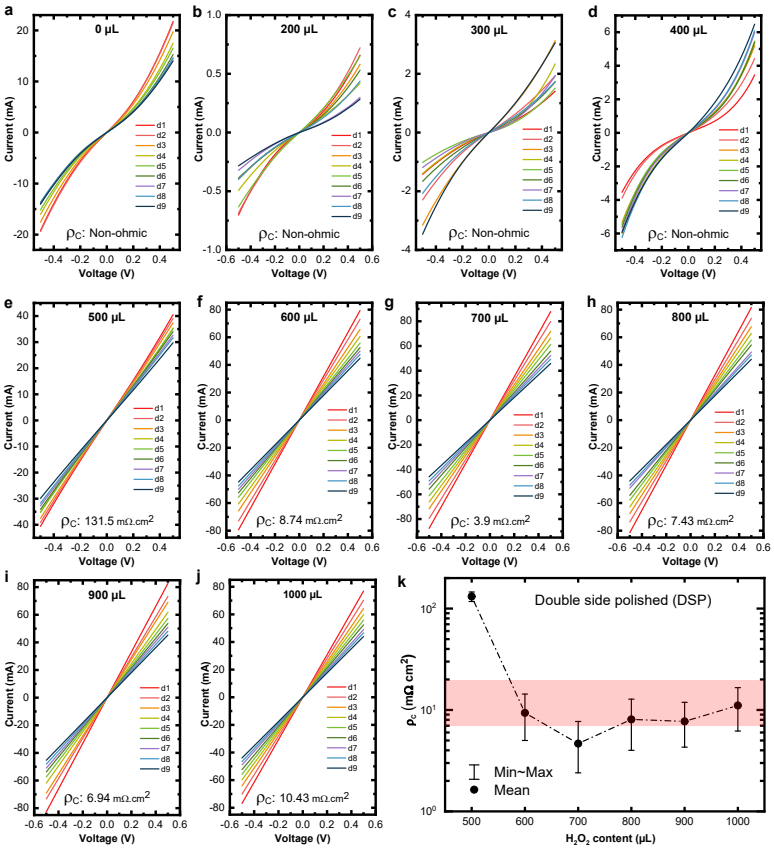

Figure S7. a–j) Dark current–voltage (I–V) curves and the extracted mean contact resistivity of the samples coated by M-TiO_x precursor solutions with different H_2O_2 contents. k) The trace of extracted ρ_c range of the samples exhibiting an ohmic contact. The highlighted region defines the ρ_c range of the n-Si/LiF_x/Al contact as a control sample. (All samples were prepared on HF-pretreated DSP-(CZ) n-type c-Si substrates (1–3 Ω cm, 280 µm))

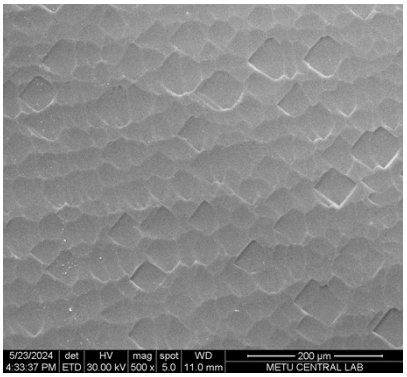

Figure S8. The top-view SEM image of the chemically etched substrate used for the fabrication of passivation and contact resistivity test samples.

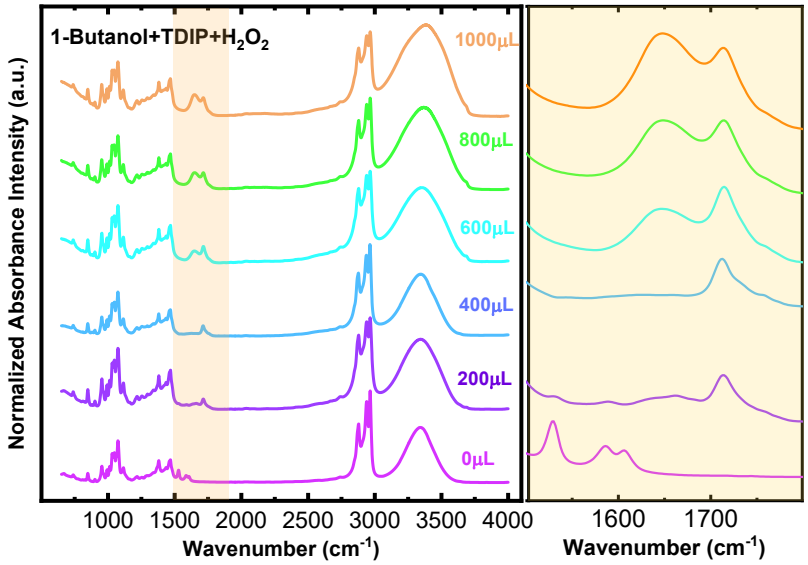

Figure S9. The ATR-FTIR absorption spectrum of the M-TiO_x precursor solutions treated by varying contents of H_2O_2 before dilution. The highlighted region (1500 – 1800 cm^{-1}) in the full absorption spectrum (650 – 4000 cm^{-1}), is magnified on the right side of the relevant figure.

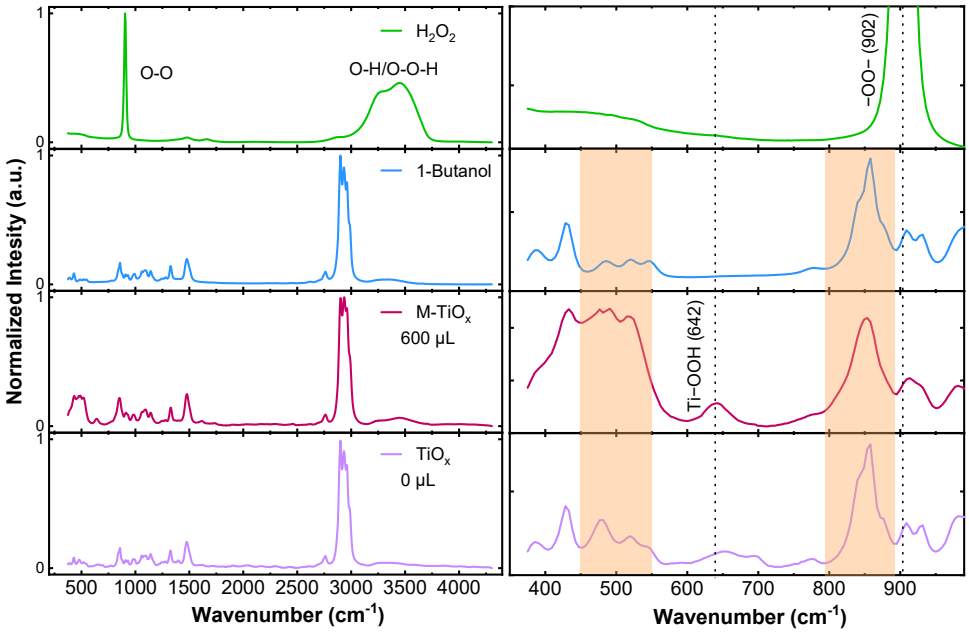

Figure S10. The Raman spectrum of the solvents composing the TiO_x precursor solution and their mixtures. Because of its high concentration (75 wt. % in isopropanol), the Raman spectrum of TDIP could not be obtained.

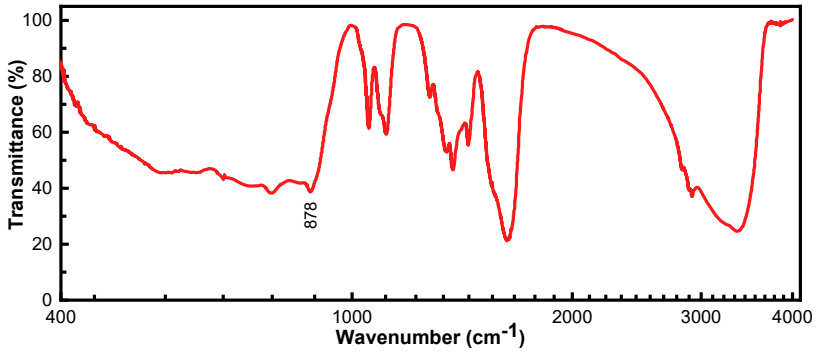

Figure S11. The transmission FTIR spectrum of the titanium-peroxo powder pellet.

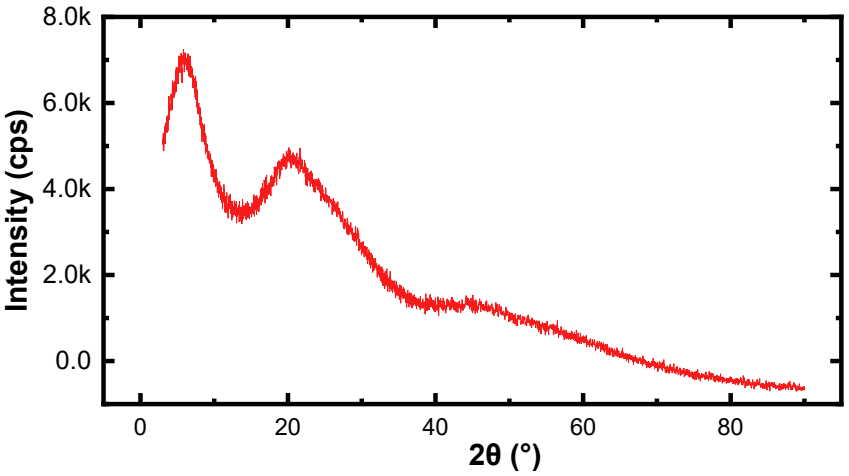

Figure S12. The XRD pattern of the titanium-peroxo powder.

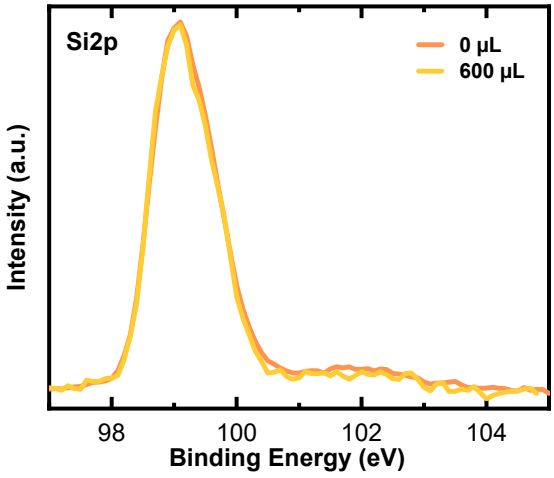

Fig. S13. The Si2p core-level XPS spectra of unmodified and modified samples.

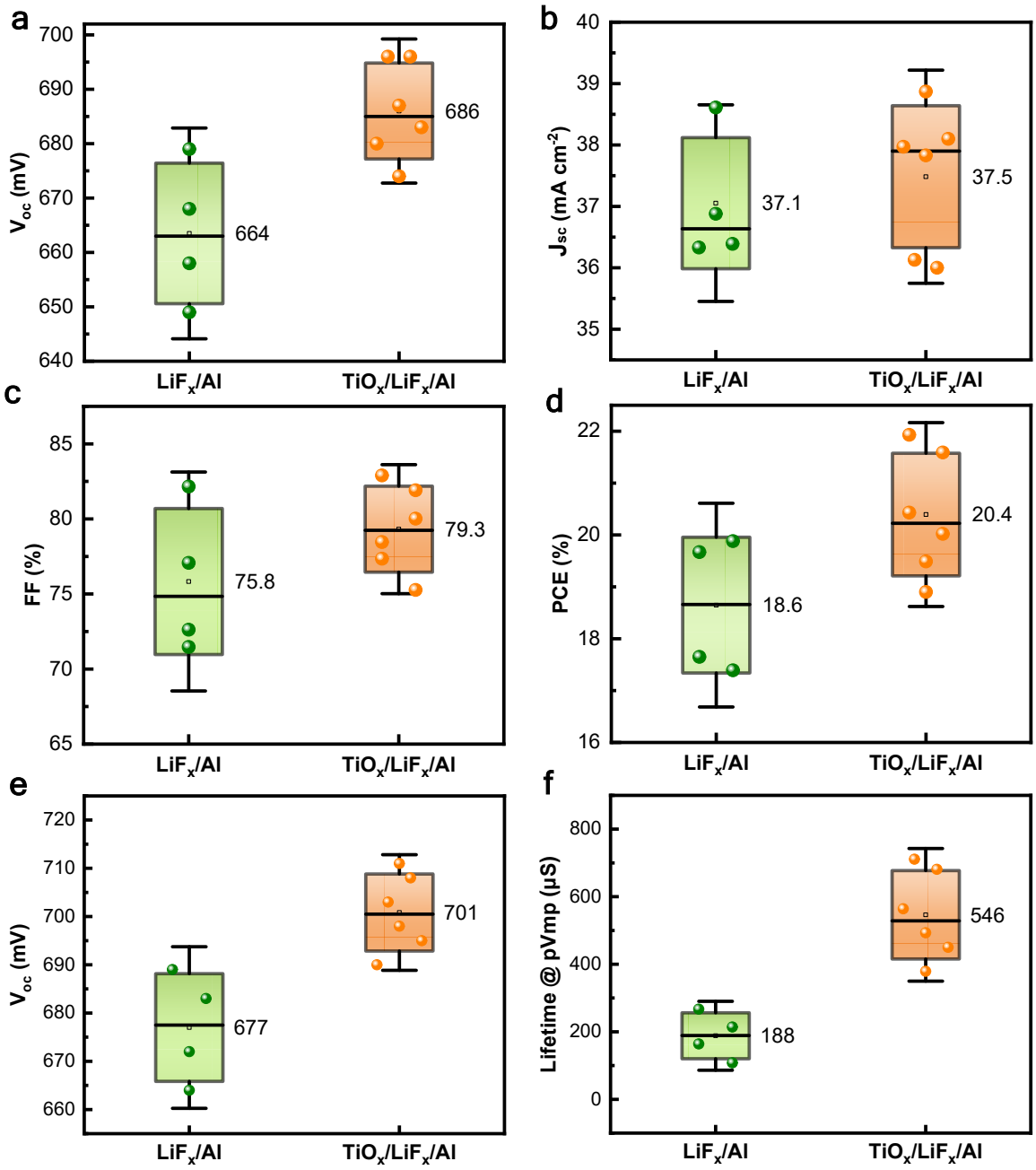

Figure S14. Statistical distribution and corresponding mean value of PV parameters for devices with LiF$_x$/Al (green), and M-TiO$_x$/LiF$_x$/Al (orange) rear contacts, fabricated in different batches and extracted by a–b) light J–V, and e and f) Suns–V_{oc} measurements.

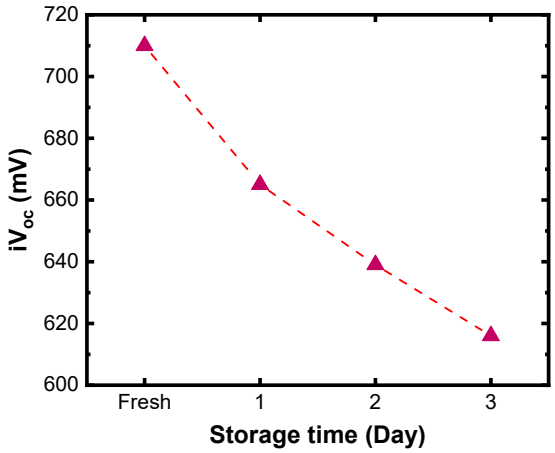

Figure S15. Variation of the iV$_{oc}$ as a function of storage time under ambient air (20–30 °C, 40–50% relative humidity).

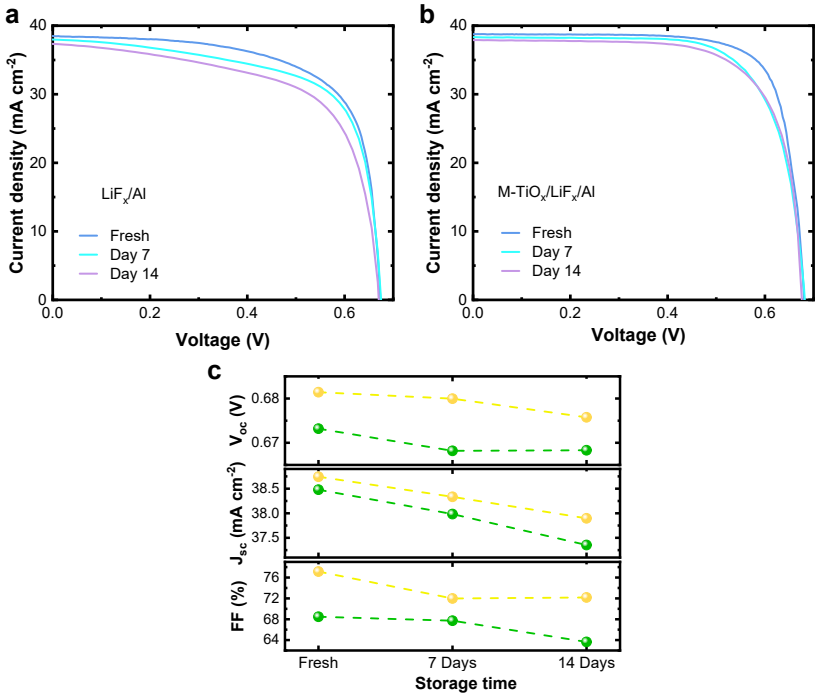

Figure S16. Corresponding a) and b) J–V curves, and c) PV metrics of data points illustrated in Figure 5e for unencapsulated devices with LiF$_x$/Al and M-TiO$_x$/LiF$_x$/Al rear contacts over storage time under ambient air. (20–30 °C, 40–50% relative humidity)

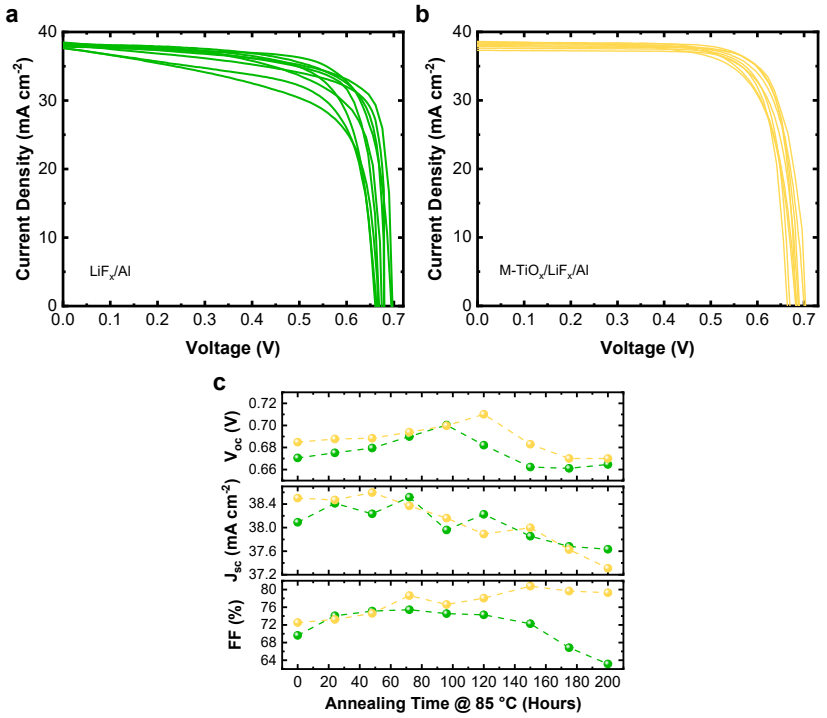

Figure S17. Corresponding a) and b) J–V curves, and c) PV metrics of data points illustrated in Figure 5f for unencapsulated devices with LiF_x/Al and M-TiO_x/LiF_x/Al rear contacts over annealing time at 85 °C on a hotplate under ambient air. (20–30 °C, 40–50% relative humidity)

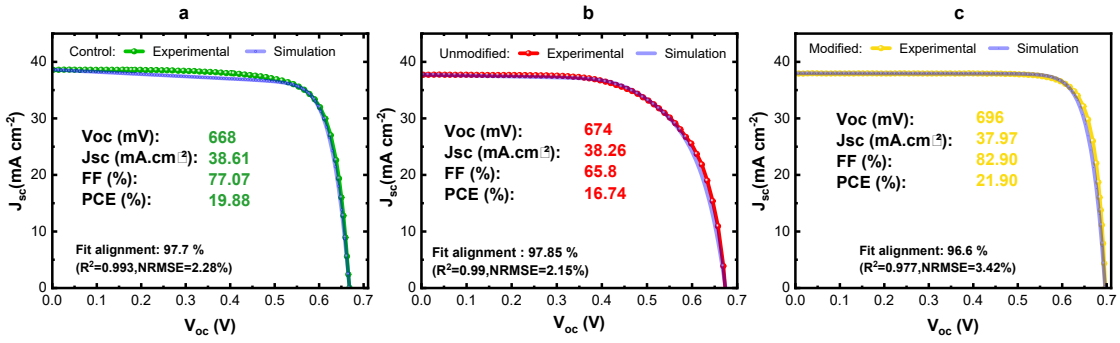

Figure S18. Experimental and SCAPS-simulated J-V of a) control, b) unmodified, and c) modified devices.

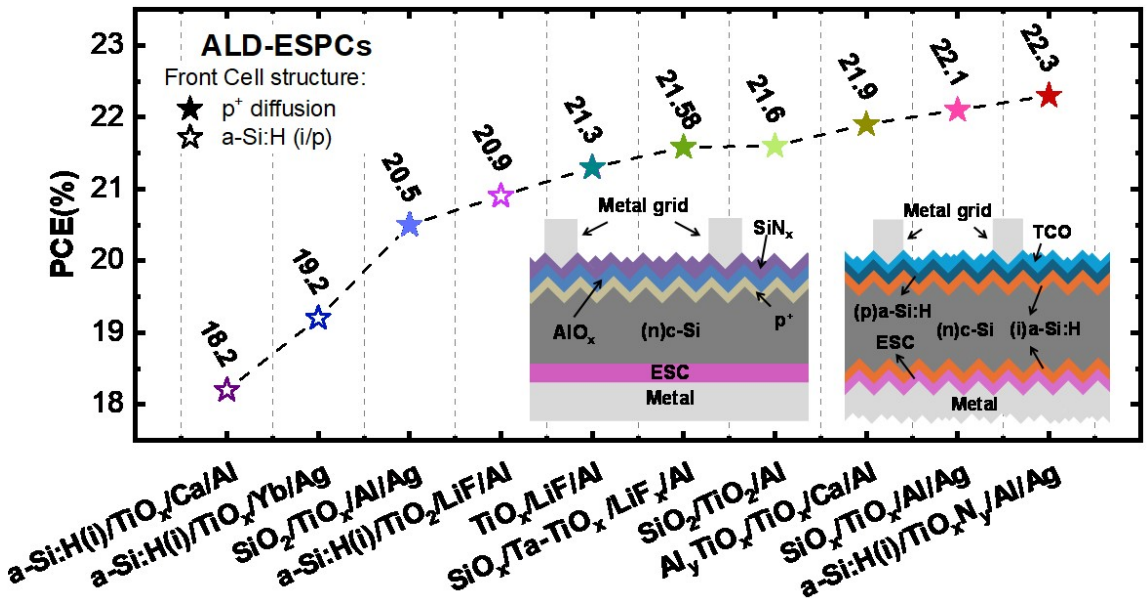

Figure S19. Previously reported pristine and dopped TiO_x-based full-area rear contacts as ESPC fabricated by ALD technique. (note that the open and closed icons represent the PCEs achieved by cells with a-Si:H(i)/a-Si:H(p)/ITO and $p^+/Al_2O_3/SiN_x$ front cell structure, respectively) For more information refer to **Table S5**.

Table S1. The assignment of peaks detected in the ATR spectra is shown in Figure S9.

Wavenumber (cm^{-1})	Group
1528	C=C, acac-Ti
1586	C=O, acac-Ti
1606	C=O, acac-enol
1722	C=O, acac- keto
1738	C=O
1640	O-H bending
1655	C=C/C=O stretching
1713	(OH)-C=O

Table S2: Global SCAPS settings and contacts

Geometry, Scan, Illumination	
Illumination	From left (front contact), AM1.5G, 1 sun, 300K.
Series / Shunt $\Omega \cdot cm^2$	$R_s = Variable$; $R_{sh} = Variable.$
Contact optical filters	Transmission values: $T_{no\ TiOx}$= 0.854, $T_{unmodified}$= 0.884, $T_{modified}$= 0.863, (used as a flat front-side loss proxy). [1]
Scaps contact mapping	
Left contact (front)	$Ag/Al_2O_3/SiNx$; Flatband.[2]
SRVs ($cm.s^{-1}$)	$S_{n=} 1 \times 10^3$, $S_{p=} 1 \times 10^7$ [3]
Right contact (Rear)	Al; Work function $\Phi = 4.3\ eV$ [4]. $\Phi_{eff\ TiOx} = 3.4$ $\Phi_{eff\ no\ TiOx} = 3$ *
SRVs ($cm.s^{-1}$)	$S_{n=} 1 \times 10^7$, $S_{p=} 1 \times 10^3$ [3]

* Effective work functions were chosen to take the effect of LiF_x and TiO_x on the rear contact into account.

Table S3: Layer parameters

Layer / parameter	P^+ **c-Si** (emitter)	**n c-Si** (bulk)	TiO_x (Unmodified)	TiO_x (Modified)	LiF_x
Thickness (μm)	0.1	140	0.01	0.017	0.001
Bandgap $E_g\ (eV)$	1.12	1.12	3.65	3.73	10
Electron affinity $\chi\ (eV)$	4.05	4.05	3.6	4.2	$\chi_{above\ layer}$
Dielectric permittivity ε_r	11.7	11.7	10	10	10
Density of states (cm^{-3})	$N_C = 2.8 \times 10^{19}$ $N_V = 1 \times 10^{19}$	$N_C = 2.8 \times 10^{19}$ $N_V = 1 \times 10^{19}$	$N_C = 1 \times 10^{18}$ $N_V = 1 \times 10^{18}$	$N_C = 1 \times 10^{18}$ $N_V = 1 \times 10^{18}$	$N_C = 1 \times 10^{20}$ $N_V = 1 \times 10^{20}$
Thermal velocities v_{th} ($cm.s^{-1}$)	$1 \times 10^7\ (n,p)$	$1 \times 10^7\ (n,p)$	$1 \times 10^7\ (n,p)$	$1 \times 10^7\ (n,p)$	$1 \times 10^7\ (n,p)$
Mobilities ($cm^2.V^{-1}.s^{-1}$)	$\mu_n = 1200$ $\mu_p = 500$	$\mu_n = 1250$ $\mu_p = 500$	$\mu_n = 25$ $\mu_p = 10$	$\mu_n = 25$ $\mu_p = 10$	$\mu_n = 1$ $\mu_p = 1$
Doping (cm^{-3})	$N_A = 1 \times 10^{19}$ $N_D = 0$	$N_A = 0$ $N_D = 4 \times 10^{15}$	$N_A = 0$ $N_D = 1 \times 10^{18}$	$N_A = 0$ $N_D = 1 \times 10^{18}$	$N_A = 0$ $N_D = 1 \times 10^7$
Bulk SRH density of recombination: N_t (cm^{-3})	1×10^{12}	5.3×10^{11}	none	none	none
Bulk SRH cross sections: σ_n, σ_p (cm^2)	$\sigma_n = 1 \times 10^{-15}$ $\sigma_p = 1 \times 10^{-15}$	$\sigma_n = 1 \times 10^{-15}$ $\sigma_p = 1 \times 10^{-15}$	$none$	none	none
Bulk SRH defect energy level: E_t (eV)	0.56 above E_V	0.56 above E_V	none	none	none
Reference(s)	[5–7]	[6,8–10]	[11–13]	[11,12]	[14]

Table S4: Interface profile

Structure	**No** TiO_x	TiO_x (Unmodified)		TiO_x (Modified)	
Rear Interface / **Parameter**	Defect 1 (Neutral)	Defect 1 (Donor)	Defect 2(Neutral)	Defect 1(Donor)	Defect 2(Neutral)
Energy reference E_t	single at 0.60 eV (above highest E_V)	single at 0.10 eV (below the lowest E_c)	single at 0.60 eV (above highest E_V)	single at 0.10 eV (below the lowest E_c)	single at 0.60 eV (above highest E_V)
Capture cross-sections (cm^2) [15,16]	$\sigma_n = 1 \times 10^{-15}$ $\sigma_p = 1 \times 10^{-15}$	$\sigma_n = 1 \times 10^{-15}$ $\sigma_p = 1 \times 10^{-22}$	$\sigma_n = 1 \times 10^{-15}$ $\sigma_p = 1 \times 10^{-15}$	$\sigma_n = 1 \times 10^{-15}$ $\sigma_p = 1 \times 10^{-22}$	$\sigma_n = 1 \times 10^{-15}$ $\sigma_p = 1 \times 10^{-15}$

Table S5. Summary of n-type silicon solar cells structure and PV outputs incorporating ALD-deposited pristine and dopped TiO_x-based full-area rear contacts as ESPC.

Rear contact scheme	Front contact scheme	V_{oc} [*mV*]	J_{sc} [*mA cm^{-2}*]	FF [%]	PCE [%]	Year	Institution	Reference No.
a-Si:H(i)/TiO_x/Ca/Al	a-Si:H (i/p)	711	35.1	72.9	18.2	2018	KU Leuven	[17]
a-Si:H(i)/TiO_x/Yb/Ag	a-Si:H (i/p)	723	33.8	78.6	19.2	2019	KU Leuven	[18]
SiO_2/TiO_x/Al/Ag	p^+ diffusion	650	39.5	80.0	20.5	2016	ANU	[19]
a-Si:H(i)/TiO_2/LiF/Al	a-Si:H (i/p)	713	37.5	78.1	20.9	2018	UC Berkeley	[20]
TiO_x/LiF/Al	p^+ diffusion	659.6	40.8	79.2	21.3	2020	SJTU-ANU	[21]
SiO_x/Ta-TiO_x/LiF_x/Al	p^+ diffusion	653.5	39.76	83.07	21.58	2024	JOU	[22]
SiO_2/TiO_2/Al	p^+ diffusion	676	39.6	80.7	21.6	2016	ANU	[23]
$Al_y$$TiO_x$/$TiO_x$/Ca/Al	p^+ diffusion	665	40.78	80.8	21.9	2022	ANU	[24]
SiO_x/TiO_x/Al/Ag	p^+ diffusion	674	39.8	82.5	22.1	2017	ANU-KAUST	[25]
a-Si:H(i)/TiO_xN_y/Al/Ag	p^+ diffusion	698	39.5	80.8	22.3	2020	SIEMIS- KAUST	[26]

REFERENCES

1 D. Wu, R. Jia, W. Ding, C. Chen, D. Wu, W. Chen, H. Li, H. Yue and X. Liu, *J. Semicond.*, 2011, **32**, 094008.
2 M. Burgelman, P. Nollet and S. Degrave, *Thin Solid Films*, 2000, **361–362**, 527–532.
3 A. G. Aberle, *Prog. Photovolt: Res. Appl.*, 2000, **8**, 473–487.
4 R. M. Eastment and C. H. B. Mee, *J. Phys. F: Met. Phys.*, 1973, **3**, 1738–1745.
5 N. F. Ramli, S. Sepeai, N. F. M. Rostan, N. A. Ludin, Mohd. A. Ibrahim, M. A. M. Teridi and S. H. Zaidi, Zlín, Czech Republic, 2017, p. 020006.
6 E. Akoto, V. Isahi, V. Odari, C. Maghanga and F. Nyongesa, *Results in Optics*, 2023, **12**, 100470.
7 R. Md. Moinuddin, M. Hasan, M. Rahaman and K. S. Islam, *AIP Advances*, 2024, **14**, 085126.
8 M. Rahmouni, A. Datta, P. Chatterjee, J. Damon-Lacoste, C. Ballif and P. Roca I Cabarrocas, *Journal of Applied Physics*, 2010, **107**, 054521.
9 A. Richter, F. Werner, A. Cuevas, J. Schmidt and S. W. Glunz, *Energy Procedia*, 2012, **27**, 88–94.
10 S. S. Li and W. R. Thurber, .
11 N. R. Pochont, Y. R. Sekhar, K. Vasu and R. Jose, *Molecules*, 2022, **27**, 7927.
12 A. Usman and T. Bovornratanaraks, *ACS Omega*, 2024, acsomega.4c04505.
13 S. B. Tekin, S. Almalki, H. Finch, A. Vezzoli, L. O'Brien, V. R. Dhanak, S. Hall and I. Z. Mitrovic, *Journal of Applied Physics*, 2023, **134**, 084503.
14 M. Q. Khokhar, S. Q. Hussain, D. P. Pham, S. Lee, H. Park, Y. Kim, E.-C. Cho and J. Yi, *Energies*, 2020, **13**, 1635.

15 C. Hu and W. G. Oldham, *Applied Physics Letters*, 1979, **35**, 636–639.
16 J. T. Ryan, A. Matsuda, J. P. Campbell and K. P. Cheung, *Applied Physics Letters*, 2015, **106**, 163503.
17 J. Cho, J. Melskens, M. Debucquoy, M. Recamán Payo, S. Jambaldinni, T. Bearda, I. Gordon, J. Szlufcik, W. m. m. Kessels and J. Poortmans, *Progress in Photovoltaics: Research and Applications*, 2018, **26**, 835–845.
18 J. Cho, J. Melskens, M. R. Payo, M. Debucquoy, H. S. Radhakrishnan, I. Gordon, J. Szlufcik, W. M. M. Kessels and J. Poortmans, *ACS Appl. Energy Mater.*, 2019, **2**, 1393–1404.
19 X. Yang, P. Zheng, Q. Bi and K. Weber, *Solar Energy Materials and Solar Cells*, 2016, **150**, 32–38.
20 J. Bullock, Y. Wan, Z. Xu, S. Essig, M. Hettick, H. Wang, W. Ji, M. Boccard, A. Cuevas, C. Ballif and A. Javey, *ACS Energy Lett.*, 2018, **3**, 508–513.
21 W. Wang, J. He, D. Yan, C. Samundsett, S. P. Phang, Z. Huang, W. Shen, J. Bullock and Y. Wan, *Solar Energy Materials and Solar Cells*, 2020, **206**, 110291.
22 L. Zhang, J. Qiu, H. Cheng, Y. Zhang, S. Zhong, L. Shi, H. Yin, R. Tong, Z. Sun, W. Shen, X. Song and Z. Huang, *Solar Energy Materials and Solar Cells*, 2024, **266**, 112703.
23 X. Yang, Q. Bi, H. Ali, K. Davis, W. V. Schoenfeld and K. Weber, *Advanced Materials*, 2016, **28**, 5891–5897.
24 M. M. Shehata, P. Phang, R. Basnet, Y. Yin, F. Kremer, G. Bartholazzi, G. G. Andersson, D. H. Macdonald and L. E. Black, *Solar RRL*, 2022, **6**, 2200550.
25 X. Yang, K. Weber, Z. Hameiri and S. De Wolf, *Progress in Photovoltaics*, 2017, **25**, 896–904.
26 X. Yang, Y. Lin, J. Liu, W. Liu, Q. Bi, X. Song, J. Kang, F. Xu, L. Xu, M. N. Hedhili, D. Baran, X. Zhang, T. D. Anthopoulos and S. De Wolf, *Advanced Materials*, 2020, **32**, 2002608.